aring talka and a same or of electronic packaging/article-pdf/14/1/3031003/6395275/ep_141_03_031003/pdf?casa_token=4PEgZNINT6UAAAAA:xbXe2uthQqYuBoZxb0hMluncmKCzwClVUNdf9vTDhAO3dGcEl9kUS0005wAevG9oBwkXzflw by University of Texas At Arlington, Satyam Saini

Jimil M. Shah¹

Department of Mechanical and Aerospace Engineering, University of Texas at Arlington, Arlington, TX 76019 e-mail: jimil.shah@mavs.uta.edu

Abel Misrak

Department of Mechanical and Aerospace Engineering, University of Texas at Arlington, Arlington, TX 76019

Dereje Agonafer

Department of Mechanical and Aerospace Engineering, University of Texas at Arlington, Arlington, TX 76019

Mike Kaler

Mestex, A Division of Mestek, Inc., 4830 Transport Drive, Dallas, TX 75247

Identification and Characterization of Particulate Contaminants Found at a Data Center Using Airside Economization

Contamination due to the use of airside economizer has become a major issue that cost companies revenue. This issue will continue to rise as server components become smaller, densely packed, and as companies move into more polluted environments. Contaminants with small particles less than 10 µm are not noticeable; yet, these particles are most likely to get to areas where they can cause damage. Dust from different sources and suspended in air settles on surfaces of electrical components. The dust mainly contains two components: salts and metallic particles. The salts may be neutral or corrosive and the nature of the salt depends on the deliquescent humidity. For metallic particles, surveys are performed in various data centers in order to determine the limits in terms of weight per unit area and particle size distribution. It is necessary to first identify those contaminants that directly affect the information technology (IT) equipment in the data center. In this research, a real-world data center utilizing airside economization in an ANSI/ISA classified G2 environment was chosen for the study. Servers were removed and qualitative study of cumulative corrosion damage was carried out. The particulate contaminants were collected from different locations of a server and material characterization was performed using scanning electron microscopy (SEM), energy dispersive spectrometer (EDS), and Fourier transform infrared spectroscopy (FTIR). The analysis from these results helps to explain the impact of the contaminants on IT equipment reliability. [DOI: 10.1115/1.4043481]

1 Introduction

Reliability of printed circuit boards (PCBs) depends upon the environmental conditions in which it is operating. The operating condition is defined by temperature, relative humidity, and contaminants in the surrounding air. There are two main failure modes for PCBs and components: open circuits due to corrosion and short-circuit caused by creep corrosion of copper terminals. Moreover, the rate of PCB failures has increased since 2006, due to the use of lead-free solders in the PCBs enforced by European Union RoHS directive [1]. Reduction of lead-based solders has given rise to copper creep corrosion, consequently causing electronic failures of PCBs. Similarly, corrosion of silver terminals of surface mount resistors has also given rise to failures caused by open circuiting. Although information technology (IT) component manufacturers have designed equipment that overcome these issues, it has been difficult to address the short-circuit issues caused by the settled particulate matter in humid environments. There has been no tangible evidence of failures besides the physical particles that are seen at the failure sites [2,3].

Short-circuit failure modes are generally common in IT equipment located in Asian countries. Due to a high level of fine particulate contaminants in the atmospheric air and increased use of free cooling methods, the occurrence of short-circuit failure mode has elevated. The sources of the particulate matter in the ambient air are both natural as well as human made. Particle contaminants have two categories: contaminants smaller than 2.5 micrometer are categorized as "fine particles," while the rest are categorized as coarse.

¹Corresponding author.

Contributed by the Electronic and Photonic Packaging Division of ASME for publication in the JOURNAL OF ELECTRONIC PACKAGING. Manuscript received November 1, 2018; final manuscript received March 14, 2019; published online May 8, 2019. Assoc. Editor: Wei Li.

Sources of fine particles include exhausts from motor vehicles and diesel particulate matter (DPM). Fine particles can further be divided into categories. Primary fine particles are directly emitted from sources such as forest fires, volcanoes, and construction sites. On the other hand, secondary fine particles, making most of the atmospheric pollutants, are introduced through natural photochemical reactions in the atmosphere. Nitrogen oxides and sulfurs produced by power plants and industries react with fine (<0.1 μ m) carbonaceous particles in complex, multistage processes, producing nitric and sulfuric acids. Ammonium salts mainly neutralize these acids. Sulfates and nitrates are also found mainly in fertilizers or resulting from biological decays. Lastly, coarse particles within the range of 2.5–15 μ m-including sea salts, artificial fibers, and pollens result from soil and mineral erosion or biological flaking [4–8].

In this research, a real-world data center utilizing airside economization in an ANSI/ISA classified G2 environment was chosen for the study. Servers were removed, and qualitative study of cumulative corrosion damage was carried out as shown in Refs. [9] and [10]. The particulate contaminants were collected from different locations of a server and material characterization was performed using Scanning electron microscopy (SEM), energy dispersive spectrometer (EDS), and Fourier transform infrared spectroscopy (FTIR). The data analysis of their results determines the grain size and elements in the contaminants. These data are very useful to understand the implications of contaminants on the IT equipment reliability.

2 Site Description

The samples for this study were collected from a research data center of around 25 kW IT load utilizing air side economization with direct and indirect evaporative cooling located in the industrial area of Dallas, TX. Direct/indirect evaporative cooling and/or

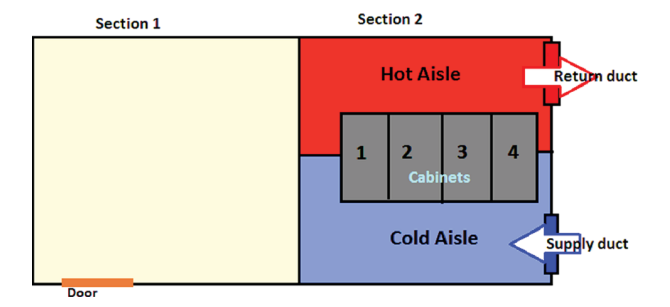


Fig. 1 Airflow Pattern inside the IT pod

return air and/or mixing of return air with outside air methods were used for the extreme environmental conditions; otherwise, free air-cooling methodology was applied if the environmental condition allowed it. The servers were arranged in the racks such that the cool inlet air entered directly toward the servers from the front to the cold aisle and provide effective cooling. The constant direction of airflow was ensured by the louver angle. Figure 1 summarizes the airflow pattern within the IT pod [9,10].

2.1 Physical Environment: Temperature and Relative Humidity. Figure 2 shows the psychrometric chart regions based on A1 allowable region as per ASHRAE environmental envelope for the cooling unit installed at the IT pod [11]. With given specifications of the unit, steps are taken to modify outside air and bring it to the acceptable region.

Further, typical meteorological year 3 data were obtained from a nearby weather center in the Dallas/Fort Worth area. The Bin data analysis provided an estimate of the number of hours the research IT pod could use air-side economizer allowing for the increased usage of free air-cooling method. The analysis

Table 1 Particulate matter and sources [9,10]

Contaminant	Source				
Zink whiskers	Zinc coated information and communications				
	technology equipment, steel building studs				
Tin whiskers	Components and products				
THI WHISKEIS	having electroplated tin				
Oxide flake off	Magnetic media				
Natural and artificial fibers	Paper, cardboard, etc.				
Water soluble ionic salt	Chemical reactions				
Sulfates, nitrate, sea salts	Transported by wind				
Lime dust with water	Concrete material				
Dust	Farm, especially during ploughing				
Toner dust	Toner				
Smoke	Cigarette, transported by wind				
Cellulose fragments	Traditional ceiling tiles and spaces				
Synthetic rubbers	Belt drive and pully				

concluded that there is a significant availability of outside air for free air-cooling application [9,10].

Next, the operating trend data of cold aisle temperature-humidity for the previous two years was analyzed. It provided an opportunity to correlate the hours of operation and its implications on the reliability of the system. Moreover, the daily analysis of cold aisle temperature and relative humidity was carried out. Data were collected for multiple days at different periods of operations. The daily analysis concluded that there were no significant variations in the temperature and the relative humidity with respect to temperature; hence, the temperature can be considered as constant for throughout the day. The analysis of the temperature and relative humidity on a monthly basis established that the unit was operated under the ASHRAE class A1 allowable region that has the lower and upper limits of A1 dry bulb temperature (59–89 °F) and relative humidity (20%–80%) for the maximum period in the past two years [9,10].

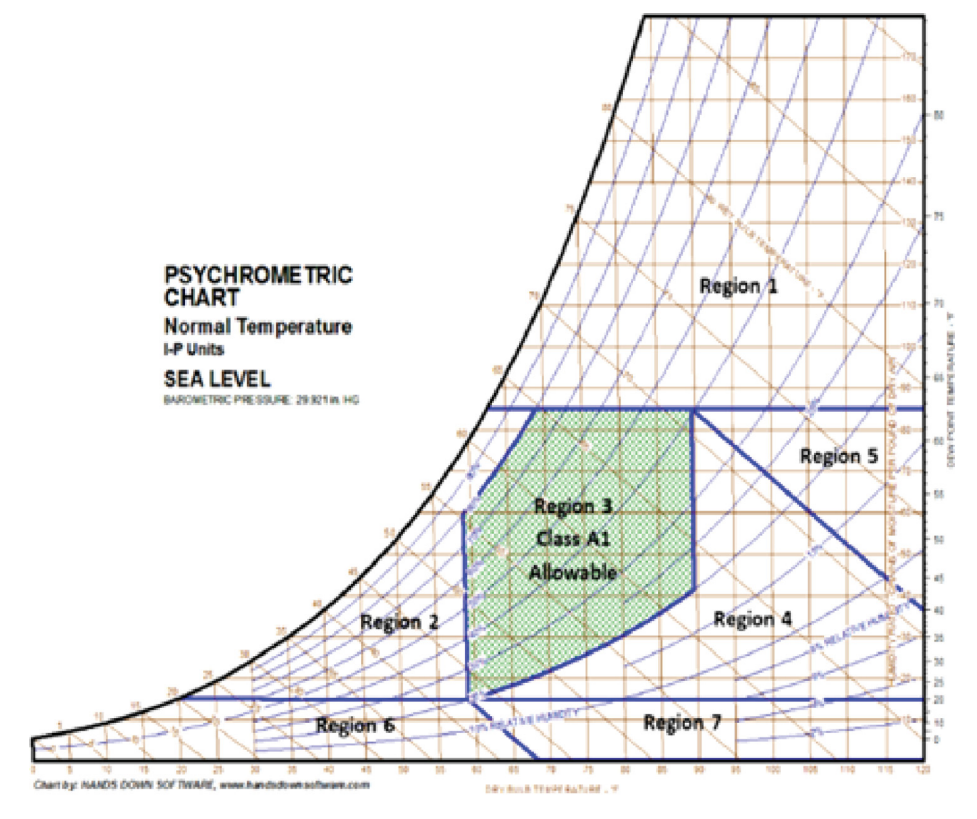


Fig. 2 Psychrometric chart regions based on A1 allowable region

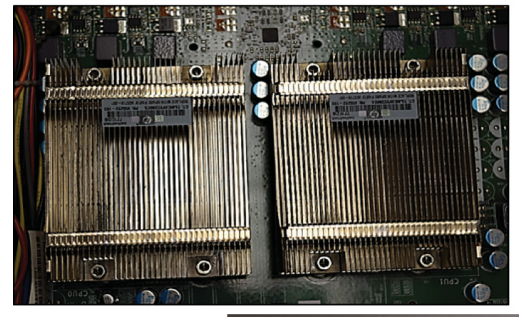






Fig. 3 Lodged dust at the different locations of the test server

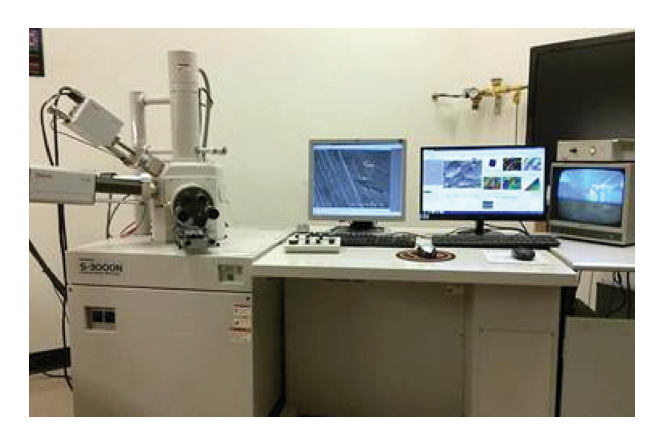


Fig. 4 Hitachi S-3000N variable pressure SEM with a thermionic source (W gun)



om https://asmedigitalcollection asme org/electronicpackaging/article-pdf/14/13/031003/6395275/ep_141_03_031003/6395275/ep_141_03_031003/e395275/ep_141_03_031003/e395275/ep_141_03_031003/e395275/ep_141_03_031003/e395275/ep_141_03_031003/e395275/ep_141_03_031003/e395275/ep_141_03_031003/e395275/ep_141_03_031003/e395275/ep_141_03_031003/e395275/ep_141_03_031003/e395275/ep_141_03_031003/e395275/ep_141_03_031003/e395275/ep_141_03_031003/e395275/ep_141_03_031003/e395275/ep_141_03_031003/e395275/ep_141_03_031003/e395275/ep_141_03_031003/e395275/ep_141_03_031003/e395275/ep_141_03_031003/e395275/ep_141_03_031003/e395275/ep_141_03_031003/e395275/ep_141_03_031003/e395275/ep_141_03_031003/e395275/ep_141_03_031003/e395275/ep_141_03_031003/e395275/ep_141_03_031003/e395275/ep_141_03_031003/e395275/ep_141_03_031003/e395275/ep_141_03_031003/e395275/ep_141_03_031003/e395275/ep_141_03_031003/e395275/ep_141_03_031003/e395275/ep_141_03_031003/e395275/ep_141_03_031003/e395275/ep_141_03_031003/e395275/ep_141_03_031003/e395275/ep_141_03_031003/e395275/ep_141_03_031003/e395275/ep_141_03_031003/e395275/ep_141_03_031003/e395275/ep_141_03_031003/e395275/ep_141_03_031003/e395275/ep_141_03_031003/e395275/ep_141_03_031003/e395275/ep_141_03_031003/e395275/ep_141_03_031003/e395275/ep_141_03_031003/e395275/ep_141_03_031003/e395275/ep_141_03_031003/e395275/ep_141_03_031003/e395275/ep_141_03_031003/e395275/ep_141_03_031003/e395275/ep_141_03_031003/e395275/ep_141_03_031003/e395275/ep_141_03_031003/e395275/ep_141_03_031003/e395275/ep_141_03_031003/e395275/ep_141_03_031003/e395275/ep_141_03_031003/e395275/ep_141_03_031003/e395275/ep_141_03_031003/e395275/ep_141_03_031003/e395275/ep_141_03_031003/e395275/ep_141_03_031003/e395275/ep_141_031003/e395275/ep_141_031003/e395275/ep_141_031003/e395275/e

Fig. 6 CrC 100 sputtering system used for coating the nonconductive samples with silver



Fig. 5 Hitachi S-4800 II FE SEM with cold field emission source $\,$



Fig. 7 Sample holder with the silver-coated sample

2.2 Physical Environment: Particulate and Gaseous Contamination. The ambient air that entered the data center was filtered using minimum efficiency reporting value 11 filters. For the initial six months, the modular data center used lower quality filters. As the data center was in the industrial area, the main sources for the contaminants were transportation exhausts and gas



Fig. 8 Thermo Nicolet 6700 FTIR spectrometer

welding particles. Table 1 summarizes the sources of different particulates [9,10]. The severity level of the site for gaseous contaminants was determined to G2 as per ANSI/ISA 71.04–1985 standard by performing corrosion classification coupon experiment as mentioned in Refs. [12] and [13].

3 Procedure

A server was removed from the research data center and qualitatively studied for cumulative corrosion damage [9,10]. Figure 3 shows the lodged dust at different locations of the test server, i.e., heat sinks, fans, and server lid (inside). The dust samples were collected from those locations and different material characterization experiments (SEM, EDS, and FTIR) were performed.

3.1 Scanning Electron Microscopy. Scanning electron microscopy is an advanced form of microscopy that uses high-voltage electrons with the wavelength as short as 0.1 Å. Though

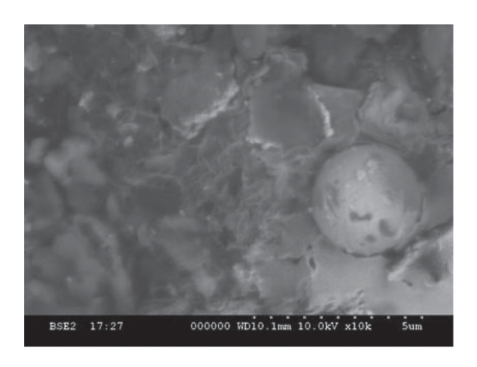
SEM technique is expensive, it is one of the desired methods of material characterization as it produces images with high magnification, resolution, and larger depth of field. SEM is used to obtain topographical, morphological, compositional, and crystallographic information. Both electrically conducting and nonconducting samples can be studied using SEM. For nonconducting samples, tests are performed under low vacuum or the sample is coated with silver.

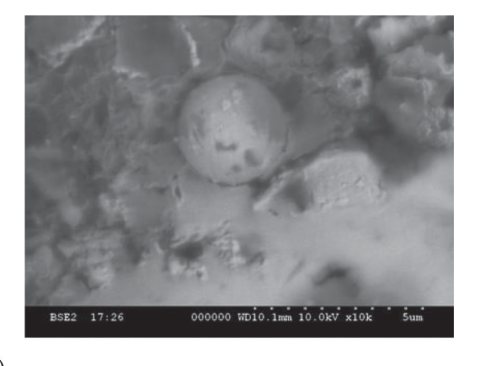
There are two types of signal electrons used for SEM imaging that result from elastic and inelastic scattering of electrons due to the interaction of probe electrons and sample. The elastically scattered electrons produce backscattering electrons (BSEs), while the inelastic scattering produces secondary electrons (SEs). In this study, both SEs and BSEs were used to obtain high-resolution images. Two SEMs were used for this test: Hitachi S-3000N variable pressure SEM with a thermionic source (W gun) (Fig. 4) and Hitachi S-4800 II field emission (FE) SEM with cold field emission source (Fig. 5).

The Hitachi S-3000N variable pressure-scanning electron microscope (VP-SEM) uses a tungsten gun for electron source. This equipment was used to obtain SE images at $\times 500, \times 10k,$ and $\times 20k$ magnification, and BSE images at $\times 10k$ for the COMPO, TOPO, and 3D modes. Some results of VP-SEM have been provided in the results section. High-resolution images obtained using S 4800 II FE SEM (shown in Fig. 5) were obtained at $\times 8k, \times 20k, \times 200k, \times 220k, \times 350k,$ and $\times 500k.$

3.1.1 Sample Preparation. Contaminants from the server shown in Fig. 3 were collected. Since the contaminants were expected to be nonconductive, they were placed on a carbon tape and coated with silver using the CrC 100 sputtering system shown in Fig. 6. Figure 7 shows the sample holder with the silver-coated sample.

After placing the sample (Fig. 7) in the SEM machine, and obtaining the desired vacuum, images were obtained at different





(a)

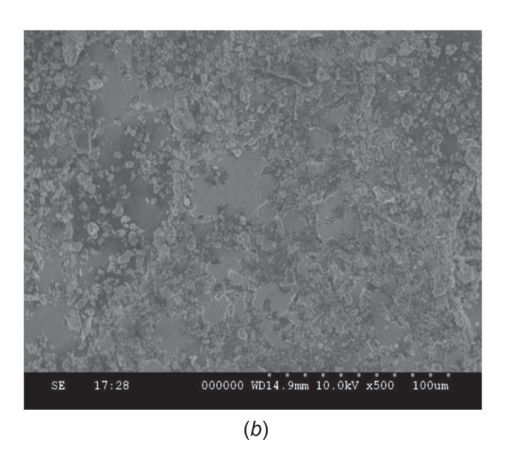


Fig. 9 (a) Back Scatter images in COMPO mode at ×10k and (b) SE images ×500

3.2 Energy Dispersive Spectrometer. The EDS technique was used to identify the different elements found in contaminant

samples. X-ray energy-dispersive spectrometer (XEDS) was developed in the late 1960s and is available as an option on transmission electron microscope and SEM. For this experiment, the EDS attached on the Hitachi S-3000N variable pressure SEM was used.

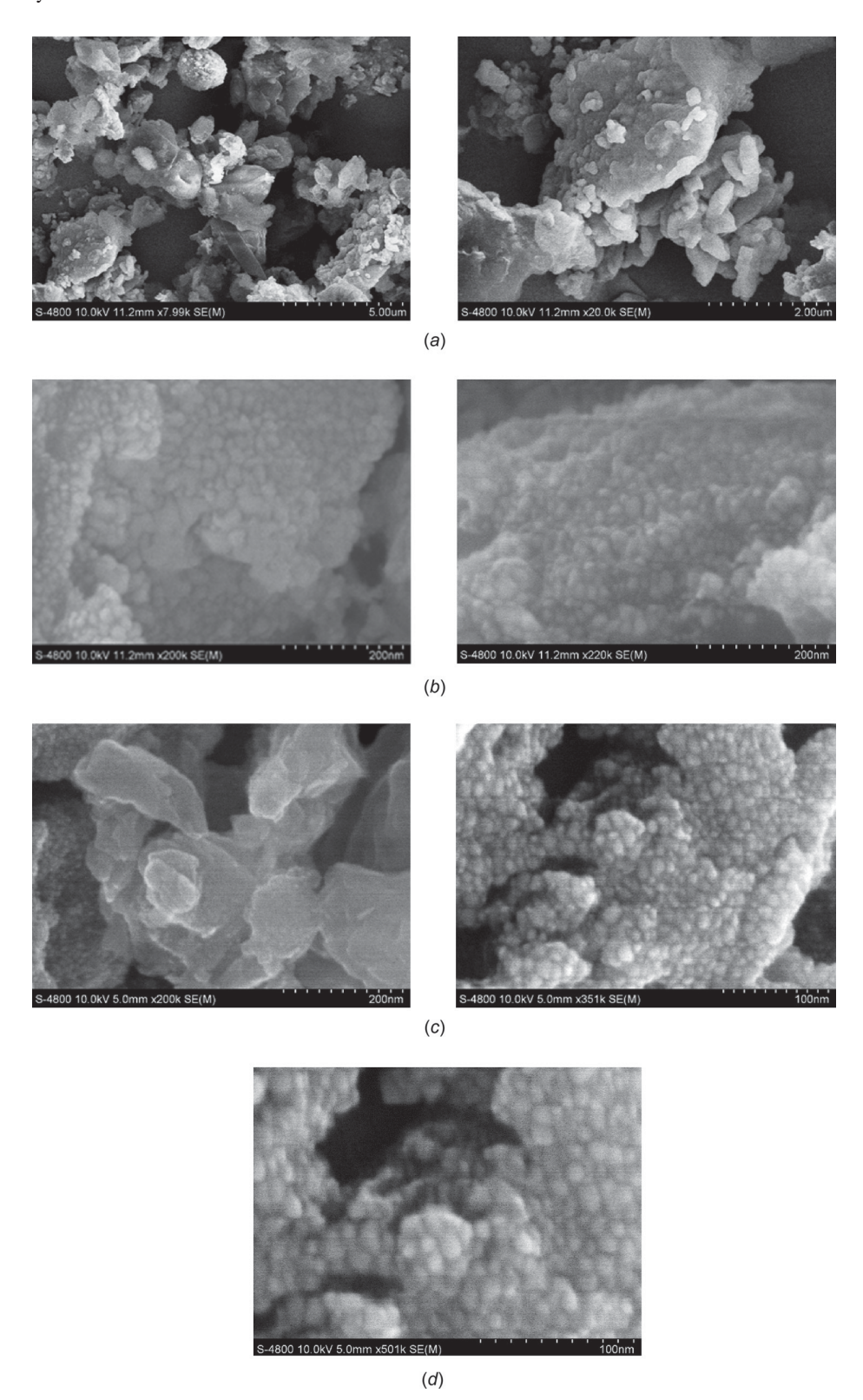


Fig. 10 (a) SE images at \times 8k (left) and \times 20k (right) at 11.2 mm working distance (WD), (b) SE images at \times 200k (left) and \times 220k (right) at 11.2 mm WD, (c) SE images at \times 200k (left) and \times 350k (right) at 5 mm WD, and (d) SE image at \times 500k at 5 mm WD

om https://asmedigitalcollection asme org/electronicpackaging/article-pdf/14/13/031003/6395275/ep_141_03_031003/6395275/ep_141_03_031003/e395275/ep_141_03_031003/e395275/ep_141_03_031003/e395275/ep_141_03_031003/e395275/ep_141_03_031003/e395275/ep_141_03_031003/e395275/ep_141_03_031003/e395275/ep_141_03_031003/e395275/ep_141_03_031003/e395275/ep_141_03_031003/e395275/ep_141_03_031003/e395275/ep_141_03_031003/e395275/ep_141_03_031003/e395275/ep_141_03_031003/e395275/ep_141_03_031003/e395275/ep_141_03_031003/e395275/ep_141_03_031003/e395275/ep_141_03_031003/e395275/ep_141_03_031003/e395275/ep_141_03_031003/e395275/ep_141_03_031003/e395275/ep_141_03_031003/e395275/ep_141_03_031003/e395275/ep_141_03_031003/e395275/ep_141_03_031003/e395275/ep_141_03_031003/e395275/ep_141_03_031003/e395275/ep_141_03_031003/e395275/ep_141_03_031003/e395275/ep_141_03_031003/e395275/ep_141_03_031003/e395275/ep_141_03_031003/e395275/ep_141_03_031003/e395275/ep_141_03_031003/e395275/ep_141_03_031003/e395275/ep_141_03_031003/e395275/ep_141_03_031003/e395275/ep_141_03_031003/e395275/ep_141_03_031003/e395275/ep_141_03_031003/e395275/ep_141_03_031003/e395275/ep_141_03_031003/e395275/ep_141_03_031003/e395275/ep_141_03_031003/e395275/ep_141_03_031003/e395275/ep_141_03_031003/e395275/ep_141_03_031003/e395275/ep_141_03_031003/e395275/ep_141_03_031003/e395275/ep_141_03_031003/e395275/ep_141_03_031003/e395275/ep_141_03_031003/e395275/ep_141_03_031003/e395275/ep_141_03_031003/e395275/ep_141_03_031003/e395275/ep_141_03_031003/e395275/ep_141_03_031003/e395275/ep_141_03_031003/e395275/ep_141_03_031003/e395275/ep_141_03_031003/e395275/ep_141_03_031003/e395275/ep_141_03_031003/e395275/ep_141_03_031003/e395275/ep_141_03_031003/e395275/ep_141_031003/e395275/ep_141_031003/e395275/ep_141_031003/e395275/e

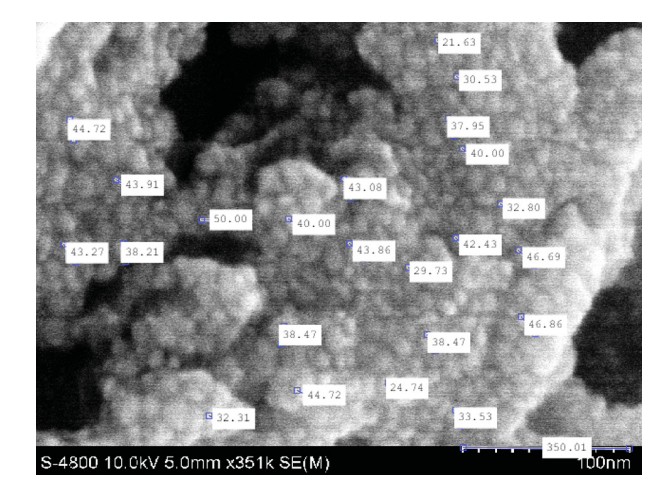


Fig. 11 The size of the different contaminants measured using analysis tool on MATLAB

To perform an EDS study, a larger field of view of the sample is needed. Thus, a lower magnification was selected ($\times 150$). After the alignment and stigmation were corrected, the beam current was increased to $60\,\mathrm{nA}$. Selected parameters such as magnification, beam current, voltage, walking distance, and EDS detector position were entered under Microanalysis. After making sure the dead time did not exceed 40%, the scan was performed to identify the elements in the sample.

3.3 Fourier Transform Infrared Spectroscopy. The vibration spectroscopy was used to analyze molecular structure by examining the interaction between infrared light and nuclear vibrations in molecules. FTIR detects the molecular vibrations by measuring the absorption of infrared light. Although this approach can be used to study both organic and inorganic materials, metallic materials cannot be studied using FTIR because of their strong reflective property.

Thermo Nicolet 6700 FTIR spectrometer along with the smart iTR accessory shown in Fig. 8 was used to study the powder samples collected from the server locations shown in Fig. 3. For both the transmission and absorption measurements, the following parameters were selected:

Number of scans: 32

Resolution: 4

Range: 4000–620 cm⁻¹

After collecting the background, the sample was placed in the FTIR machine and the data were collected.

4 Results and Data Analysis

4.1 Scanning Electron Microscopy

- 4.1.1 VP-Scanning Electron Microscopy Results. Figures 9(a) and 9(b) show some of the results obtained from VP-SEM.
- 4.1.2 FE-Scanning Electron Microscopy Results. Figures 10(a)-10(d) show the results obtained from FE-SEM. Results clearly show that the shape of found contaminants is spherical.
- 4.1.3 Data Analysis–Scanning Electron Microscopy. Scanning electron microscopy results were analyzed to obtain two sets of data. First, the SEM SE images were used to obtain the average grain size for the contaminants. Second, The EDS data were analyzed to obtain the compositional analysis of the contaminants. To determine the particulate size, the image analysis tool in MATLAB was used. Some of the results are given in Fig. 11.

Size of the various grains identified previously in Fig. 10(c) as measured by MATLAB units is given by the following list: $\{21.63, 30.53, 44.72, 37.95, 43.91, 43.08, 40.00, 50, 40, 32.8, 43.27,$

Table 2 Possible functional groups present in the contaminant sample

Peaks	Wavenumber (1/cm)	Possible group O–H (H bonded), stretching			
1	3391.				
2	2359.5	N/A			
3	1621.3	Metal-H stretching			
4	1415.1	C-O-H bending			
5	1004.0	C-O stretching			
6	873.8	C–H bending			
7	797.5	=C $-$ H and $=$ CH2			
8	668.2	O-H bend (out of plane)			

38.21, 43.86, 42.43, 46.69, 29.73, 38.47, 38.47, 46.86, 44.72, 24.74, 32.31, 33.53}. Using the scale at the bottom of Fig. 10(d) and converting the values to nanometers, the average particulate size is determined to be 11.03 ± 2.09 nm. The results clearly indicate that the found particulates are the ultra-fine particles.

4.2 Energy Dispersive Spectrometer

4.2.1 Results. Figures 12(a) shows the results obtained from the spectral analysis showing the locations of the various elements identified in one location of the sample.

Figures 12(b) and 12(c) show the identified elements from EDS measurement results. Similar measurements were carried out at six different locations of the sample. The matrix correction factor (ZAF), which considers the atomic number, X-ray absorption, and X-ray fluorescence, was applied separately for each element in the sample.

4.2.2 Data Analysis–Energy Dispersive Spectrometer. The EDS data was analyzed to obtain the compositional analysis of the contaminants.

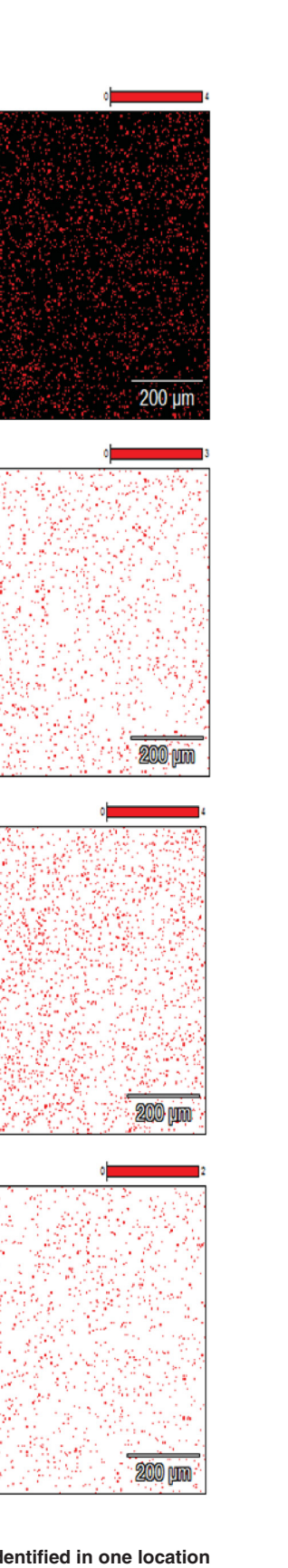
Figure 13 shows the average element weight of six locations of the sample. It shows that carbon composes 47.63% of the contaminant sample. The carbon tape used in the base of the sample may be responsible for the high percentage of carbon; however, based on previous qualitative studies on contaminants from the same site, it can be concluded that there is a high carbon content in the contaminants.

4.3 Fourier Transform Infrared Spectroscopy

- 4.3.1 Results. Figures 14(a) and 14(b) show the absorbance and transmission data collected using the FTIR, respectively. Figure 14(c) show the results obtained after performing the search in the FTIR database. The result shows low percent match with different compounds. Identifying the details of these compounds will be part of future work.
- 4.3.2 Data Analysis. Fourier transform infrared spectroscopy was performed to analyze the molecular structure and compounds of found particulates. Based on the results obtained, it can be concluded that the contaminant sample contained different compounds. Unfortunately, these compounds could not be identified from the FTIR search database. Therefore, online tools that provided chemical group classification as a function of the wavenumber were used to identify the possible chemical groups that are present in the contaminant sample. The sources available from Michigan State University and Chemistry LibreTexts were used to determine Table 2, respectively [14,15].

5 Conclusion

Motor vehicle exhaust from diesel-fueled vehicles is very polluting to the environment. DPM is the particulate component of diesel exhaust that includes diesel soot (carbon) and aerosols. DPM can take the form of individual particles or aggregates, with



Si K

om https://asmedigitalcollection asme org/electronicpackaging/article-pdf/14/13/031003/6395275/ep_141_03_031003/6395275/ep_141_03_031003/e395275/ep_141_03_031003/e395275/ep_141_03_031003/e395275/ep_141_03_031003/e395275/ep_141_03_031003/e395275/ep_141_03_031003/e395275/ep_141_03_031003/e395275/ep_141_03_031003/e395275/ep_141_03_031003/e395275/ep_141_03_031003/e395275/ep_141_03_031003/e395275/ep_141_03_031003/e395275/ep_141_03_031003/e395275/ep_141_03_031003/e395275/ep_141_03_031003/e395275/ep_141_03_031003/e395275/ep_141_03_031003/e395275/ep_141_03_031003/e395275/ep_141_03_031003/e395275/ep_141_03_031003/e395275/ep_141_03_031003/e395275/ep_141_03_031003/e395275/ep_141_03_031003/e395275/ep_141_03_031003/e395275/ep_141_03_031003/e395275/ep_141_03_031003/e395275/ep_141_03_031003/e395275/ep_141_03_031003/e395275/ep_141_03_031003/e395275/ep_141_03_031003/e395275/ep_141_03_031003/e395275/ep_141_03_031003/e395275/ep_141_03_031003/e395275/ep_141_03_031003/e395275/ep_141_03_031003/e395275/ep_141_03_031003/e395275/ep_141_03_031003/e395275/ep_141_03_031003/e395275/ep_141_03_031003/e395275/ep_141_03_031003/e395275/ep_141_03_031003/e395275/ep_141_03_031003/e395275/ep_141_03_031003/e395275/ep_141_03_031003/e395275/ep_141_03_031003/e395275/ep_141_03_031003/e395275/ep_141_03_031003/e395275/ep_141_03_031003/e395275/ep_141_03_031003/e395275/ep_141_03_031003/e395275/ep_141_03_031003/e395275/ep_141_03_031003/e395275/ep_141_03_031003/e395275/ep_141_03_031003/e395275/ep_141_03_031003/e395275/ep_141_03_031003/e395275/ep_141_03_031003/e395275/ep_141_03_031003/e395275/ep_141_03_031003/e395275/ep_141_03_031003/e395275/ep_141_03_031003/e395275/ep_141_03_031003/e395275/ep_141_03_031003/e395275/ep_141_03_031003/e395275/ep_141_031003/e395275/ep_141_031003/e395275/ep_141_031003/e395275/e

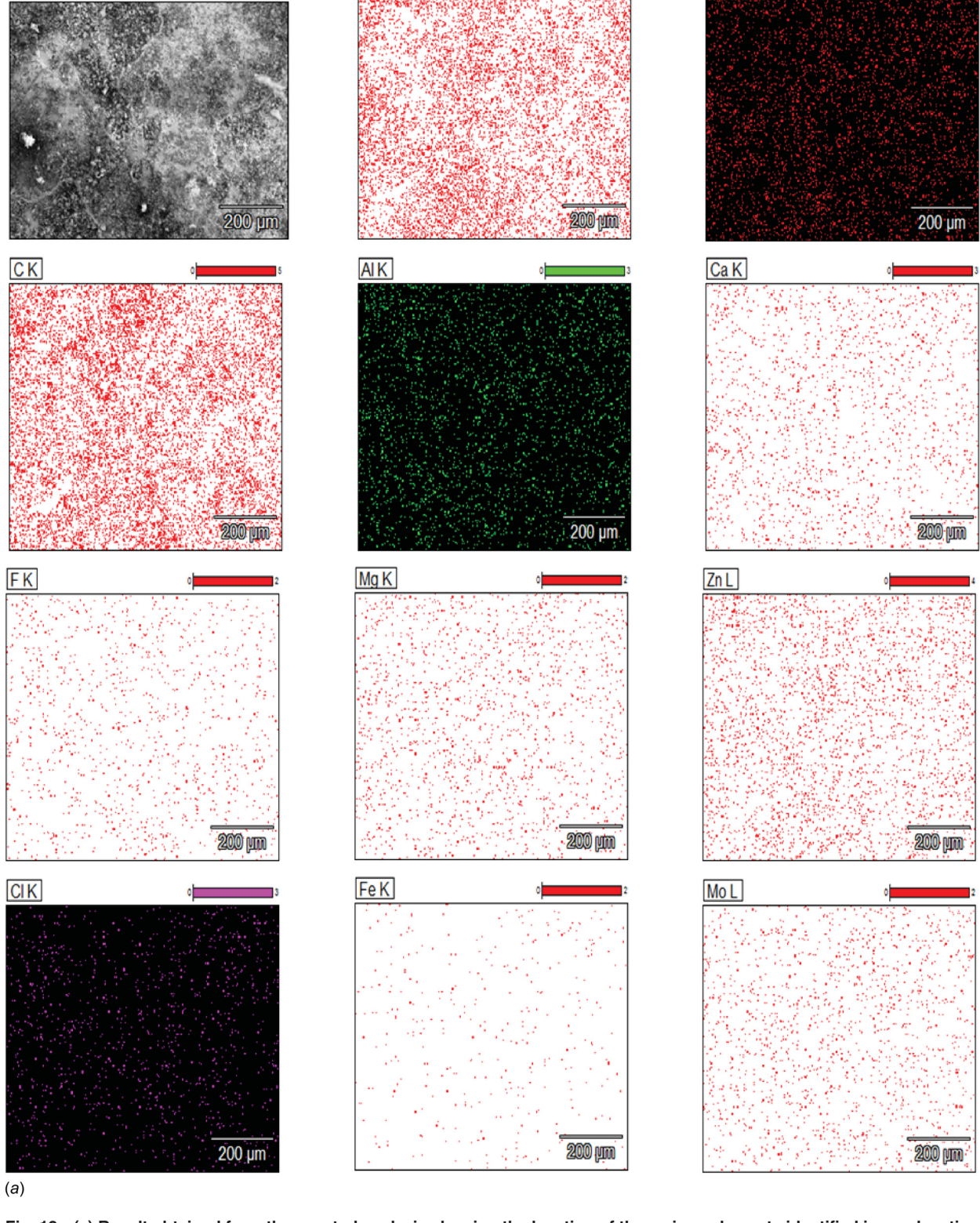
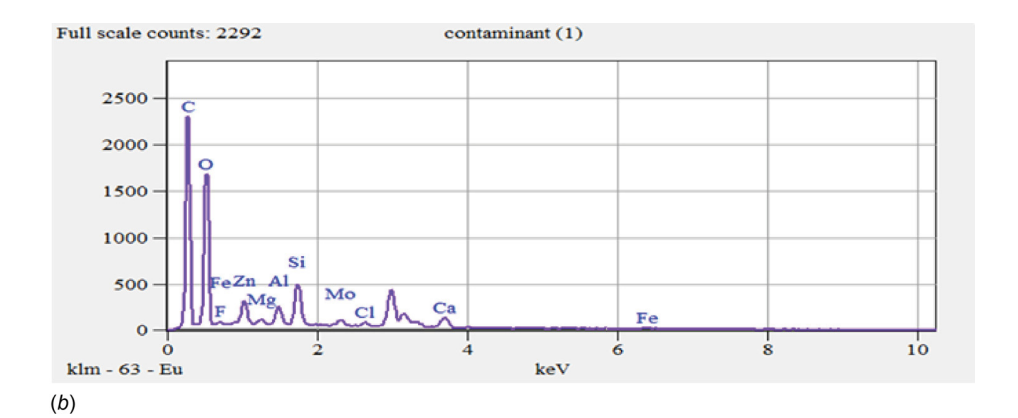


Fig. 12 (a) Result obtained from the spectral analysis showing the location of the various elements identified in one location of the sample, (b) result of the spectrum analysis of one location of the sample, and (c) result of quantitative analysis of one location of the sample

contaminant (1)



Element Line	Int. Cps/nA	Z	A		ZAF	Weight %	Weight % Error	Norm. Wt.%	Norm. Wt.% Err	Atom %	Atom % Error
CK		0.960	2.172	1.000	2.086	46.70	± 0.48	46.70	± 0.48	62.27	± 0.64
OK		0.984	2.673	1.000	2.629	27.11	± 0.52	27.11	± 0.52	27.14	± 0.52
FK		1.050	2.495	1.000	2.618	0.46	± 0.37	0.46	± 0.37	0.39	± 0.31
Mg K		1.037	1.293	0.998	1.339	0.47	± 0.07	0.47	± 0.07	0.31	± 0.05
AIK		1.072	1.172	0.997	1.254	1.94	± 0.16	1.94	± 0.16	1.15	± 0.09
Si K		1.045	1.108	0.998	1.155	5.22	± 0.16	5.22	± 0.16	2.98	± 0.09
CIK		1.112	1.037	0.997	1.149	3.19	± 0.22	3.19	± 0.22	1.44	± 0.10
Ca K		1.094	1.010	1.000	1.105	5.90	± 0.20	5.90	± 0.20	2.36	± 0.08
Fe L		1.163	1.650	0.999	1.917	0.00		0.00		0.00	± 0.00
Zn L		1.213	1.278	0.999	1.550	5.81	± 0.28	5.81	± 0.28	1.42	± 0.07
Mo L		1.333	0.993	0.997	1.320	3.20	± 0.20	3.20	± 0.20	0.53	± 0.03
Total						100.00		100.00		100.00	

Fig. 12 (Continued)

most in the invisible submicron range of $0.1\,\mu\text{m}$, also known as ultrafine particles or PM0.1. These ultrafine particles are not visible to the naked eye. The experimental site is in the industrial area and surrounded by the truck traffic. That is the biggest source for carbon particulates found inside the data center.

(c)

Particulate contamination in the data center may affect IT equipment performance as well as the reliability. This may include the performance of heat sinks, electronic and mechanical devices. Other major factors include the deliquescent relative humidity (DRH), which may humidify the particulate matter causing short-circuiting on printed circuit boards. As per the results obtained above, although filters do remove some dust particles, they are not very effective for particles of size PM2.5. Moreover, humidity conditions of about 50%–65% can cause condensation on PCBs, which allows particles to settle as time goes on. Additionally, condensation causes leakage of current around PCBs, increasing the chances for short-circuits.

Particle contamination also affects the thermal conductivity of components [9,10]. Accumulated particles create an insulating layer, which reduces heat dissipation effectiveness of the server, causing components to overheat. Similarly, magnetic particles that sweep into the system may cause damage to electric components such as fans and other rotors if they come within the magnetic field generated by such components. Further, particles that have electrically conductive properties such as carbon and other metallic substances can cause short-circuits in the electrical components. Particles with insulating properties can also settle static charges, which could affect the working of PCBs and other electrical components. Some insulating particles do absorb moisture due to humid environmental conditions and consequently increasing the chances of short-circuits. Particles with adhesive properties could attract more particles to settle on the surfaces, further increasing the detrimental effects on the components. Dust particles may become corrosive in nature by encountering various gaseous contaminants, hence causing damage to components. Lastly, fast moving particles may cause erosion to the mechanical components and can cause critical damage to their surface.

However, ultra-fine particles may take longer period to get accumulated at a particular location in a server to cause significant damages. Authors documented that there is no failure of even a single server at this site during its five years of operation. As mentioned earlier, since the study was done in an industrial area of hot and humid Dallas under harsh operating conditions, we feel comfortable that the results of this study are applicable for a much broader climate zone.

6 Future Work

In the future, similar analysis should be performed at data centers located in varying climate zones. Second, it can be inferred that the particulates found are ultra-fine. It is very difficult to trap them using the typical minimum efficiency reporting value filters

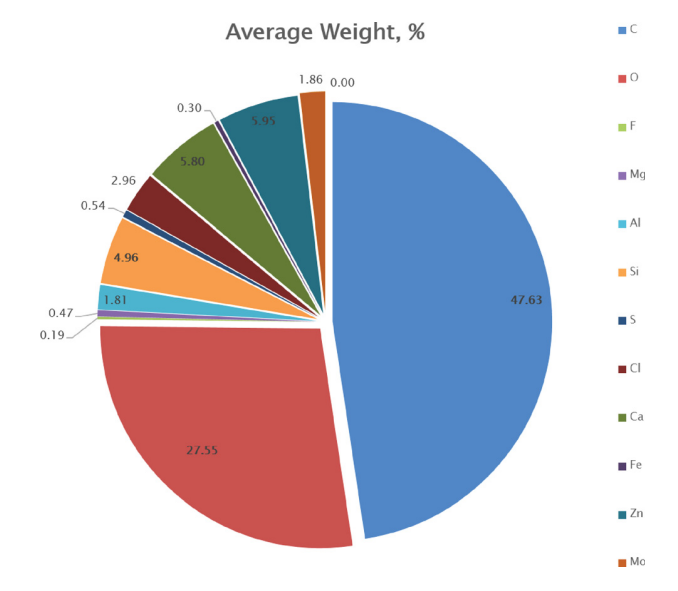
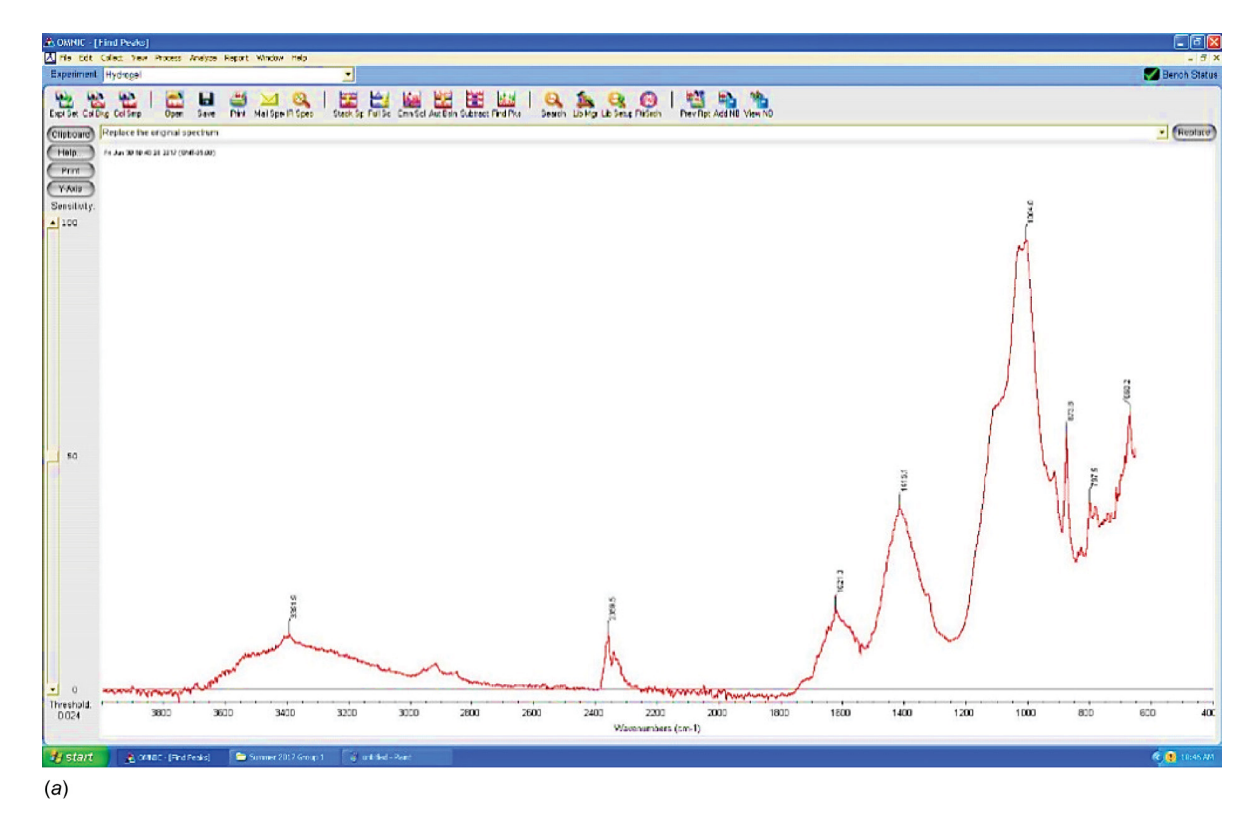


Fig. 13 Average weight of elements identified in the contaminant sample in percentage



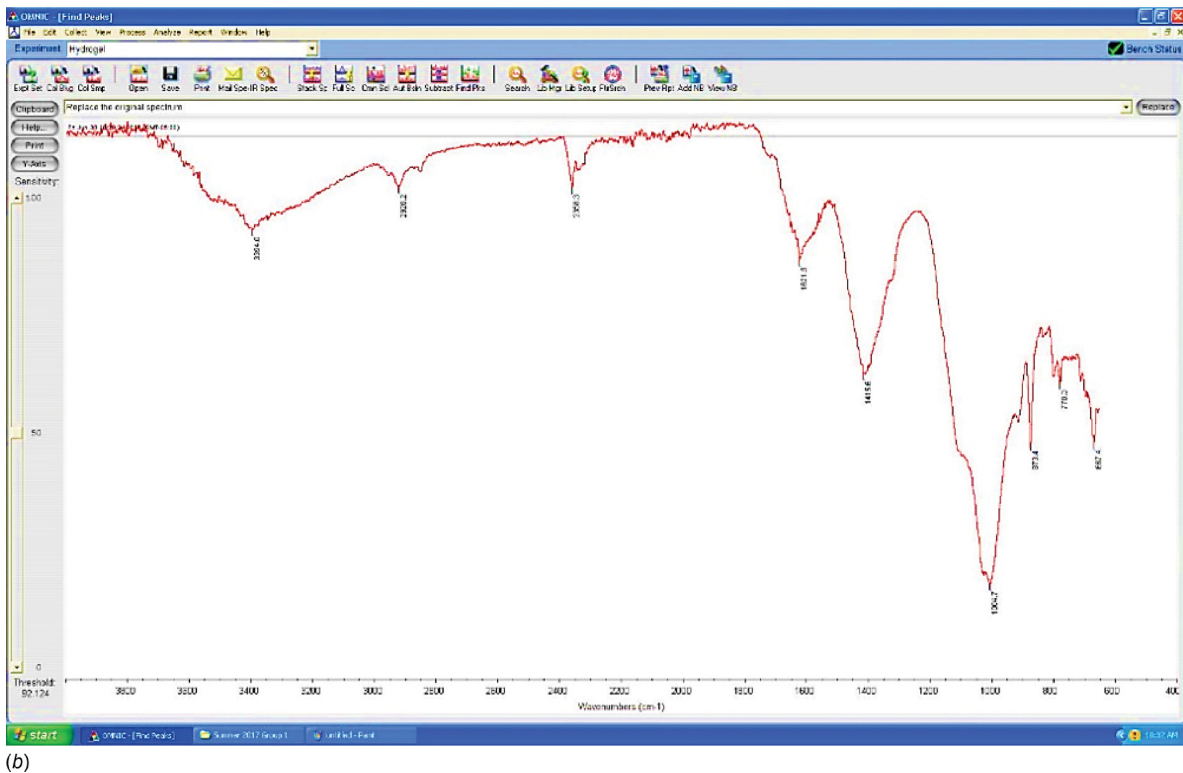


Fig. 14 (a) Absorbance data collected using FTIR, (b) transmission data collected using FTIR, and (c) result obtained after performing the search in the FTIR database

used in data centers. This type of particulates can cause intermittent failures. The DRH of these particles from real-world data centers should be studied. DRH is defined as the relative humidity at which the salt or dust particles begin the formation of a saturated

salt solution. The relative humidity of the data center should be maintained lower than the DRH of such particles. It is also dependent on the location of the contaminants in a server. Currently, authors are developing a precise and cost-effective DRH

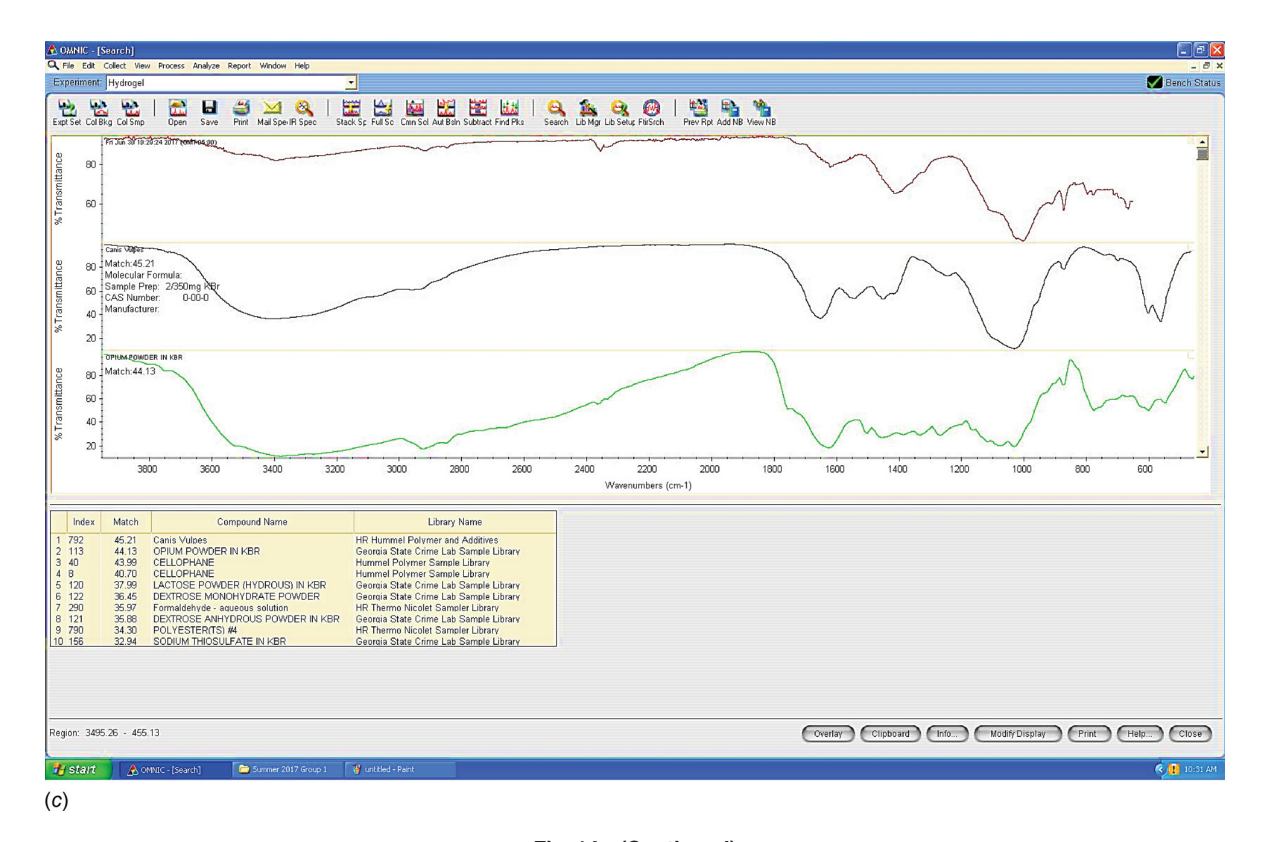


Fig. 14 (Continued)

measurement technique. Upon, the successful validation of methodology, authors will collect multiple samples from the same site and perform DRH of particulate contaminants found in a real-world data center.

Acknowledgment

This work is supported by NSF I/UCRC in Energy-Smart Electronic Systems (ES2). We would like to thank Dr. Prabjit Singh, IBM for his valuable feedback on this work. We would also like to thank Dr. Jiechao Jiang of UT Arlington's CCMB lab for his insightful comments and advices.

Funding Data

NSF (Funder ID: 10.13039/501100008982).

Nomenclature

A = differences in absorption of X-rays

 $COMPO\ mode = Composition\ mode$

F = differences in the production of secondary X-rays, or X-ray fluorescence

TOPO mode = topographic mode

Z = differences in mean atomic number

References

- [1] European Union, 2003, "Directive 2002/95/EC of the European Parliament and of the Council of 27 January 2003 on the Restriction of the use of Certain Hazardous Substances on the Electrical and Electronic Equipment Official Journal L 037," Off. J. Eur. Union, 1037, pp. 19–23.
- [2] Shah, J. M., 2016, "Reliability Challenges in Airside Economization and Oil Immersion Cooling," Master's thesis, University of Texas at Arlington, Arlington, TX.
- [3] Singh, P., Klein, L., Agonafer, D., Shah, J. M., and Pujara, K. D., 2015, "Effect of Relative Humidity, Temperature and Gaseous and Particulate Contaminations on Information Technology Equipment Reliability," ASME Paper No. IPACK2015-48176.

- [4] Burnett, W. H., Sandroff, FS., and D'Egidio, S. M., 1992, "Circuit Failure Due to Fine Dust Mode Particulate Air Pollution," 18th International Symposium for Testing and Failure Analysis (ISTFA '92), Los Angeles, CA, Oct. 17–23, pp. 329–333.
- [5] Litvak, A., Gadgil, A. J., and Fisk, W. J., 2000, "Hygroscopic Fine Mode Particle Deposition on Electronic Circuits and Resulting Degradation of Circuit Performance: An Experimental Study," Indoor Air, 10, pp. 47–56.
- [6] Fu, H., Chen, C., Singh, P., Zhang, J., Kurella, A., Chen, X., Jiang, X., Burlingame, J., and Lee, S., 2012, "Investigation of Factors That Influence Creep Corrosion on Printed Circuit Boards," SMTA Pan Pacific Microelectronics Symposium, Kauai, HI, Feb. 14–16, Paper No. PP2012_WA1.4.
- [7] Comizzoli, R. B., Frankenthal, R. P., Lobnig, R. E., Peins, G. A., Psota-Kelty, L. A., Siconolfi, D. J., and Sinclair, J. D., 1993, "Corrosion of Electronic Materials and Devices by Submicron Atmospheric Particles," Electrochem. Soc. Interface, pp. 27–33.
- [8] Song, B., Azarian, M. H., and Pecht, M. G., 2013, "Effect of the Temperature and Relative Humidity on the Impedance Degradation of Dust-Contaminated Electronics," J. Electrochem. Soc., 160(3), pp. C97–C105.
- [9] Shah, J. M., Awe, O., Agarwal, P., Akhigbe, I., Agonafer, D., Singh, P., Kannan, N., and Kaler, M., 2016, "Qualitative Study of Cumulative Corrosion Damage of IT Equipment in a Data Center Utilizing Air-Side Economizer," ASME Paper No. IMECE 2016-66199.
- [10] Shah, J. M., Awe, O., Gebrehiwot, B., Agonafer, D., Singh, P., Kannan, N., and Kaler, M., 2017, "Qualitative Study of Cumulative Corrosion Damage of Information Technology Equipment in a Data Center Utilizing Air-Side Economizer Operating in Recommended and Expanded ASHRAE Envelope," ASME J. Electron. Packag., 139(2), p. 020903.
- [11] ASHRAE Technical Committee 9.9, 2012, Thermal Guidelines for Data Processing Environments (ASHRAE Datacom Series), 3rd ed., American Society of Heating, Refrigerating, and Air-Conditioning Engineers, Atlanta, GA.
- [12] ISA, 1985, "Environmental Conditions for Process Measurement and Control Systems: Airborne Contamination," ISA-The Instrumentation Systems, and Automation Society, Research Triangle Park, NC, Standard No. ISA-71.04:1985.
- [13] ISA, 2013, "Environmental Conditions for Process Measurement and Control Systems: Airborne Contaminants," ISA-The Instrumentation Systems, and Automation Society, Research Triangle Park, NC, Standard No. ISA-71.04:2013.
- [14] Reusch, W., 2019, "Infrared Spectroscopy," Michigan State University, East Lansing, MI, accessed Mar. 3, 2019, https://www2.chemistry.msu.edu/faculty/ reusch/virttxtjml/Spectrpy/InfraRed/infrared.htm
- [15] LibreTexts, 2019, "Infrared: Interpretation," San Diego, CA, accessed Mar. 3, 2019, https://chem.libretexts.org/Core/Physical_and_Theoretical_Chemistry/Spectroscopy/ Vibrational_Spectroscopy/Infrared_Spectroscopy/Infrared%3A_Interpretation